Theoretical study of controlling multistability by parametric and stochastic modulation in the Hénon map and a fiber laser.

by

Cruz Yuliana Calderón Hermosillo

B.Sc., University of Guanajuato, 2006

A THESIS SUBMITTED IN PARTIAL FULFILMENT OF
THE REQUIREMENTS FOR THE DEGREE OF

Master of Science

(Optics)

Centro de Investigaciones en Óptica A. C.

December, 2007

© Cruz Yuliana Calderón Hermosillo 2007

Dedication

To my siblings;
José Luis,
Lucía,
Mariana and
Martín.

Acknowledgements

I would like to thank God for giving me the opportunity to study and also for being my source of wisdom, patience and strength to let me complete this program.

Thanks to CONACYT for the scholarship that give me during my master studies and for the grant by the proyect No. 46973-E.

Thanks to my family for your love despite of the distance.

Thanks to my supervisor Dr. Alexander N. Pisarchik, and Dr. Alexander V. Kir'yanov, and Dr. Evguenii Kourmychev for their observations.

Thanks to Prof. Dr. Jürguen Kurths, and Dr. Udo Shwartz, and Carolina Figueroa for their supervision and support during my stay at the Institute for Physics (University of Potsdam, Germany).

Thanks to Daniel for his support despite of the distance.

Thanks to all of my friends.

Table of Contents

List of Tables

List of Figures

List of Abbreviations.

EDFL	Erbium-doped Fiber Laser.
ESA	Excited-state absorption.
FBG	Fiber Bragg Grating.
FWHM	Full-width at half maximum.
PC	Polarization Controller.
SNB	Saddle-node Bifurcation.
SNR	Signal-to-Noise Ratio.
SR	Stochastic Resonance.
WDM	Wavelength-division multiplexer.

Abstract

In this thesis, I study theoretically the applicability of the method for controlling multistability by parametrical and stochastic modulation. The method for controlling multistability was suggested by Pisarchik and Goswami in 2000. It implies additional harmonic modulation to a system parameter that allows annihilation of undesirable attractors in a multistable system. I begin from a study of the attractor annihilation in the bistable Hénon map subject to additive noise. The Hénon map is one of the simplest dynamical systems which exhibits coexistence of attractors. First, I focus on the parameter region where two different periodic orbits coexist (period 1 and period 3) and apply additional harmonic modulation to a system parameter to destroy the period-3 attractor.

I demonstrate that additive noise can facilitate the attractor annihilation for some modulation frequencies, in the sense that an undesired attractor can be destroyed with a smaller amplitude of the control modulation. On the other hand, for other modulation frequencies noise can stabilize the attractor. In the latter case, noise induces multistability in the system with parameter modulation.

Then, I explore the parameter region in the map where a periodic orbit coexists with a chaotic orbit and study the influence of noise on attractor annihilation.

Finally, I study resonance phenomena in the volume of basins of attraction of coexisting period-1 and period-3 attractors in the Hénon map, subject to normally distributed noise added to both variables. As the noise level is increased, the volume of the basin of attraction of the period-1 attractor grows up, while the volume of the basin of the period-3 attractor drops down. At a certain level of noise the volume of the basin of the period-1 attractor reaches its maximum value.

In the second part of the thesis, I study numerically attractor annihilation in an erbium-doped fiber laser (EDFL) with three coexisting attractors. The annihilation curves are analyzed with codimensional-one and codimensional-two bifurcation diagrams. The results of this study are in good agreement with experimental results reported previously by Pisarchik *et.al.*

Chapter 1

Introduction.

Many nonlinear systems exhibit the coexistence of multiple dynamical equilibrium states (attractors) in some regions of parameter space. This phenomenon, referred to as *generalized multistability,* has been found in a variety of systems in different fields, including electronics, optics, mechanics and biology, in addition to some standard models like the Hénon map, Duffing, Rössler, van der Pol, and Lorenz equations. In such multiattractor systems a final state depends crucially on initial conditions. However, in many practical situations multistability can create inconvenience, for instance, in construction of optical devices with determined characteristics. A method for controlling multistability was suggested by Pisarchik and Goswami in 2000 [1]. The authors called up the idea of complete annihilation of undesirable attractors in order to make the system monostable. They showed that undesirable states can be destroyed by a weak periodic modulation applied to a system parameter. Later the method has been applied to control multistability in coupled Duffing oscillators [2], a time-delayed logistic map [3], and lasers [4]. The method has been realized experimentally in a CO_2 laser [1] and in a fiber laser [5].
In this thesis I study numerically the application of the method for controlling multistability to discrete and continuous systems. As a paradigm of a discrete-time dynamical system I select the Hénon map. It is one of the most studied examples of dynamical systems that exhibit chaotic behavior. The Hénon map takes a point (x, y) in the plane and maps it to a new point. The canonical Hénon map is interesting because, unlike the logistic map, its orbits are defined by a simple description. The change in the dynamical behavior of the map can be illustrated through a bifurcation diagram, which demonstrates the evolution of the map variables through different critical points where the dynamics is qualitatively changed, as a parameter is varied. It is very important for any control method to consider its robustness against noise. Noise is generally associated with hindrance, with something that is irregular and cannot be perfectly controlled. Furthermore, noise is virtually unavoidable since it is impossible to isolate a system perfectly from its environment. We are taught by conventional wisdom that the transmission

and detection of signals is hindered by noise. However, during the last two decades, the paradigm of *stochastic resonance* (SR) proved this assertion wrong: indeed, the addition of the appropriate amount of noise can boost a signal and hence facilitate its detection in a noisy environment. Due to its simplicity and robustness, SR has been implemented by mother nature on almost every scale, thus attracting interdisciplinary interest from physicists, geologists, engineers, biologists and medical doctors, who nowadays use it as an instrument for their specific purposes [6].
In stochastic resonance, the signal-to-noise ratio (SNR) is nonmonotonic with respect to noise level. This cannot occur in linear systems. Most recent studies of stochastic resonance involve bistable systems with a weak external periodic forcing [7].
As an example, I explore the noisy Hénon map, since the Hénon map is one of the simplest systems which can display generalized multistability. All the analysis is performed with MATLAB. The system dynamics is studied with time series, power spectra, bifurcation diagrams, and basins of attraction of coexisting attractors.

In the second part of thesis I study the applicability of the method for attractor annihilation to continuous system on an example of a laser system. I consider an erbium-doped fiber laser (EDFL). The advantages of these lasers are the long interaction length of pumping light with the active ions, which leads to high gain and to single-transversal-mode operation produced by a suitable choice of fiber parameters. These properties make EDFLs excellent light sources for optical communications, reflectometry, sensing, medicine, etc. Meanwhile, these lasers are quite sensitive to any external perturbation that may destabilize their normal operation. Therefore, the knowledge of the dynamic behavior of these lasers is of great importance and can be important for many applications.

From the viewpoint of nonlinear dynamics, rare-earth-doped fiber lasers, along with solid-state, semiconductor, and electric discharge CO_2 and CO lasers, belong to class-B lasers. In these class of laser, polarization is adiabatically eliminated and the dynamics can be ruled by two rate equations for field and population inversion. In spite of an impressive array of research on complex dynamics in lasers, the nonlinear dynamics of EDFLs has begun to be studied only recently. Only few papers have been devoted to a study of the nonlinear response of the EDFL to parametric modulation. The main features of the dynamic behavior of these lasers are similar to those of other class-B lasers. First, a period-doubling route to chaos was

observed by Lacot *et al.* [8] in a bipolarized two-mode EDFL with harmonic pump modulation. The authors have also developed a model based on two coherently pumped coupled lasers. Later, a quasi-periodic route to chaos was found by Sanchez *et al.* [9] in a dual-wavelength EDFL. Eventually Luo *et al.* [10] revealed the coexistence of period-doubling and intermittency routes to chaos in a pump-modulated ring EDFL. They also reported on bistability (the coexistence of two periodic attractors) in this laser. More recently, optical bistability (coexistence of a limit cycle and a fixed point) was detected by Mao and Lit [11] in the vicinity of the first laser threshold in a dual-wavelength EDFL with overlapping cavities.

Recently, the coexistence of multiple periodic attractors (generalized multistability) has been found both theoretically and experimentally in EDFLs subjected either to loss or pump modulation [2]. Many papers have been devoted to a study of self-pulsation behavior of EDFLs. Such behavior has been suggested to be due to the presence of a saturable absorber in the fiber in the form of ion pairs or pump depletion. The Q-switching behavior can also be attributed to excited-state absorption (ESA) at the lasing wavelength and to a thermo-lensing effect that is due to ESA at the pump wavelength.

In this thesis I explore the theoretical model of 1560-nm EDFL developed recently by Dr. A. V. Kiryanov [12] which displays multistability under harmonic modulation of a diode pump laser. I study laser dynamics over a wide range of frequencies and amplitudes of pump modulation. Then I apply the control technique for attractor annihilation to simulate the experiments reported in Ref. [2]. Finally, I find good agreement between the numerical and experimental results.

The thesis contains five chapters.

Chapter 1. Introduction.
Introduction contains the justification, objectives, methodology and describes the structure of the thesis.

Chapter 2. Basic concepts of nonlinear dynamics.
This chapter briefly introduces the reader to basic concepts and definitions of nonlinear dynamics, such as discrete and continuous systems, periodic orbits, attractors, bifurcations, stochastic resonance, deterministic resonance, and coherence resonance.

Chapter 3. Control of multistability in the Hénon map.
In this chapter I study the Hénon map in the parameter region where period-1 and period-3 attractors coexist, the influence of noise and parametric modulation on the coexistence of the attractors. I start with the case where noise is added to a single variable and investigate the effect of additive noise with either uniform or normal distribution. Then, I consider the case when normal noise is added to both map variables and search for the noise threshold for *attractor annihilation*. I also study volumes of the basins of attraction of the coexisting attractors in the presence of normally distributed noise. Finally, I present the dependence of the basin's volumes on noise and demonstrate the existence of a noise-induced resonance refered to as *generalized coherence resonance.*

In this chapter I also consider the range of the coexistence of period-3 and chaotic attractors and apply small harmonic modulation to the control parameter when the system stays initially in one of the states.

Chapter 4. Control of multistability in an erbium-doped fiber laser.
This chapter is devoted to a numerical study of dynamics of a multistable erbium-doped fiber laser with three coexisting attractors. I demonstrate with codimentional-one and codimentional-two bifurcation diagrams where the method for attractor annihilation can be used to control multistability in this laser.

Chapter 5. Conclusions.
This chapter contains general conclusions of the thesis.

Chapter 2

Basic Concepts of Nonlinear Dynamics.

Introduction

In this chapter I will describe briefly several concepts of nonlinear dynamics which I will use in the rest of the thesis. I will give definitions of such fundamental concepts as discret and continuous systems, periodic orbits, attractors, bifurcations, stochastic resonance, deterministic resonance, and coherence resonance.
Since the material of this chapter is standard, it can be found in many textbooks on nonlinear dynamics (see, e.g., [13, 14, 15, 16, 17, 18]).
I will give only basic descriptions of these concepts, which will be enough to understand the remaining chapters.

2.1 Definitions

Nonlinear dynamics
Dynamics is a concept that deals with a system change, i.e. with systems which evolve in time. Whether the system in question settles down to equilibrium, keeps repeating in cycles, or does something more complicated, so it is dynamics that we use to analyze the behavior. So, a dynamical system consists of a set of possible states, together with a rule that determines present states in terms of past states. Some examples of dynamical systems are swinging pendulums, bouncing balls, robot arms, reactions in a chemical process, water flowing in a stream, or an airplane in flight. In the case of the pendulum, both position and velocity vary in time, so we would focus in these states and the rules that determine how they change over time. Usually, we have a mathematical model that can be derived from a set of laws, that tell us how a real dynamical system works. The model will typically have equations that may be parameterized by time and the previous states

of the system. These equations can be used to get the future state of a dynamical system. Whenever parts of a dynamical system interfere, or co-operate, or compete, there are nonlinear interactions going on, and therefore the behavior of such systems is non-linear. We may say that linear systems do not occur very often in nature.
Thus, a rough definition of a *nonlinear dynamical system* is a system whose time evolution equations are nonlinear, that is, the dynamical variables describing the properties of the system appear in the equations in a nonlinear form, and the superposition principle does not apply.

Discrete system

There are two types of dynamical systems: discrete and continuous systems. A *discrete time system* takes the current state as input and updates its variable by producing a new state as output. Discrete time systems are called *maps*.
Mathematically a map is defined as a function whose domain (input) space and range (output) space are the same and the rule that governs a map is

$$\mathbf{x}_n = f\ (\mathbf{x}_{n-1}), \tag{2.1}$$

where the variable n stands for time and $\mathbf{x}_n$ is the state of the system in time n. The output of the rule is used as an input value for the next state. In this work we explore a discrete time dynamical system, in particular, the Hénon map, which is described as

$$\begin{aligned} x_{n+1} &= 1 - \mu x_n^2 + y_n, \\ y_{n+1} &= -J x_n, \end{aligned} \tag{2.2}$$

where x_n and y_n can be measured as time series, J is the determinant of Jacobian related to dissipation, and μ is the parameter.

Continuous time dynamical system

A dynamical system consists of a set of possible states, together with a rule that determines the present states in terms past states. In a continuous dynamical system, the governed rule is a set of differential equations and the term of a continue time dynamical system is sometimes used.
The general state equation is

$$\dot{u} = f(u), u(t_0) = u_0, \tag{2.3}$$

where $u \in D \subset R^n$, $t \in R^+$. D is an open subset of R^n.

Autonomous system
A system of differential equations of the form 2.3, in which the independent variable t does not occur explicitly is called *autonomous system.*

Nonautonomous system
Consider the following differential equation:

$$\dot{u} = f(u,t), u(t_0) = u_0, u \in D \subset R^n, t \in R^+. \tag{2.4}$$

If the right-hand side depends explicitly on time equation 2.4, it is called nonautonomous system.

Periodic equation
If in the equation 2.4 $f(u,t) = f(u,t+T)$ for $T > 0$ exist for all u and t, then equation 2.4 is said to be time periodic with period T.

Attractor
There are many different types of motion which a dynamical system can exhibit. We can define an *attractor* as an asymptotically stable fixed point or an orbit in the phase space, at which the system is attracted to.
There are many types of attractors: fixed points, limit cycles, chaotic attractors, infinite states, synchronized states, etc. Here we will define only those of them which we will use in the Hénon map.

Fixed point
If a discrete system is given by a map $f : R^n -> R^n$, the point $\mathbf{u}^* \in R^n$ is called a *fixed point* if $f(\mathbf{u}^*) = \mathbf{u}^*$.

Sometimes the fixed points are called equilibrium points or critical points.
The simplest attractor is a fixed point, which can be seen, for example, in a pendulum when friction and gravity bring the system to a halt.

Periodic orbit
We can also observe so-called *periodic orbits* of period k, defined by k points such that

$$\begin{aligned} \mathbf{x}_{i+1} &= f\ (\mathbf{x}_i), \\ \mathbf{x}_{i+2} &= f(f\ (\mathbf{x}_i)) = f\ ^2(\mathbf{x}_i), \\ &\vdots \\ \mathbf{x}_{i+k} &= f^k(\mathbf{x}_i) = \mathbf{x}_i, \end{aligned} \tag{2.5}$$

where $k > 0$.

Chaotic attractor

Chaos is an irregular behavior of a system. A chaotic attractor, is not a fixed point or a limit cycle. However, not any system that fluctuates irregularly in time represents a chaotic behavior. Chaos, as used in nonlinear dynamics, represents a behavior observed in deterministic dynamical equations. Chaotic dynamics has the additional property that small differences in initial conditions grow over time, but the dynamics is finite, and variables do not grow indefinitely. This property is often called *sensitive dependence on initial conditions*. Because of this important property, it is impossible to make accurate long term prediction about the state of the system without knowing exactly its initial state. Any minor uncertainty will be amplified so as to render actual knowledge of the state of the system is impossible. In a real system it is always impossible to know the state of the system exactly, since there always exists some uncertainty in experimental measurements.

Phase space

If the dynamical system is given by $f : R^n -> R^n, R^n$ is refered to as *phase space*. We will assume, it has the standard Euclidean structure.

Time series

In statistics and signal processing, *time series* is a sequence of data points, measured typically at successive times, spaced apart at uniform time intervals. A time series graph shows the growth of a sequence as a function of time.

Basin of attraction

Let x^* be an asymptotically stable fixed point (attractor) of map f . Then the *basin of attraction* (or the stable set) $w^s(x^*)$ of x^* is defined as the set A containing x^* such that if $x \in A$, then $f^{\,n}(x) \to x^*$ as $n \to \infty$ (i.e., the maximal set that is attracted to attractor x^*) .

Deterministic chaos

Deterministic chaos denotes the irregular or chaotic motion that is generated by nonlinear systems whose dynamical laws uniquely determine the time evolution from a knowledge of its previous history. So, deterministic chaos means that there is a definite rule with no random term governing the dynamics. In deterministic models every event or action is the inevitable result of preceding events, thus, in principle, every fact can be completely

predicted in advance. In 1892 Poincaré described mathematically that a small change in the initial conditions produced a big change on the final state of the famous three-body problem under the action of gravity.

Bifurcation

A *bifurcation* describes the qualitative changes in the set of fixed points or periodic points or other sets of dynamical interest that can be observed while a parameter of a system is varied. For example, under the variation in the parameter value, a fixed point may change from being stable to unstable, or a cycle might suddenly appear.

Saddle-node bifurcation

A saddle-node bifurcation results in the creation of two new fixed points, one stable and one unstable.

Bifurcation diagram

A *bifurcation diagram* represents the dynamical behavior of a system as a function of a control parameter. The bifurcation diagram can be constructed by repeating the following procedure: (1) Fix a value of control parameter a, (2) Fix initial conditions for variables x, (3) Calculate a map, (4) Ignore transients and plot x, (5) Increase a. A bifurcation diagram displays the birth, evolution, and the death of attracting sets.

Power spectrum

For a given signal, a *power spectrum* gives a plot of the portion of a signal's power (energy per unit time) falling within given frequency bins. The most common way of generating a power spectrum is by using a Fast Fourier Transform (FFT), but other techniques such as the maximum entropy method can also be used.

Generalized multistability

The coexistence of attractors is often called *generalized multistability*. In nonlinear systems, multiple attractors are common, and indeed there may be periodic and chaotic attractors coexisting.

Stochastic resonance

Stochastic resonance (SR) is a phenomenon of an increase of the signal-to-noise ratio (SNR) with increasing input noise in bistable or multistable nonlinear systems [19, 20].

Deterministic resonance

Deterministic resonance (or noise-free stochastic resonance) is a quite similar phenomena to SR caused by internal chaotic dynamics instead of external noise. It was discovered by Anishchenko *et al.*[21] in a simple map.

Coherence resonance

In the case of an excitable system driven by an appropriate (moderate) amount of noise, however, the trajectory of the system can become quite regular, a phenomenon known as *autonomous stochastic resonance* or *coherence resonance* [22].

Characteristic frequency of attractor

Mathematically, the *characteristic frequency* (or relaxation oscillation frequency) f_r is the eigenfrequency, i.e. the imaginary part of eigenvalues of the associated stable solution. The relaxation oscillation frequency can be also measured numerically from time series or power spectrum as a maximum system response to small-amplitude modulation.

Attractor annihilation

The method for *attractor annihilation* was suggested by Pisarchik and Goswami [1] to control generalized multistability. The method implies small harmonic parameter modulation with properly chosen frequency and amplitude.

Chapter 3

Control of multistability in the Hénon map

3.1 Coexistence of periodic orbits

Introduction
In this chapter I study the effect of additive noise in a bistable system. As an example, I explore the noisy Hénon map, first, in the parameter region where period-1 and period-3 attractors coexist. I shall show how the period-3 attractor can be either destroyed or stabilized in the presence of both periodic and stochastic modulation of different amplitudes.

3.1.1 Noise is added to one variable

In this section, I study the effect of additive noise, with either uniform or normal distribution, in the Hénon map with two coexisting periodic attractors. I find a threshold value of noise amplitude ξ, at which the period-3 attractor can be destroyed.

The noisy Hénon map can be described as

$$\begin{aligned} x_{n+1} &= 1 - \mu x_n^2 + y_n + \xi\sigma(1), \\ y_{n+1} &= -Jx_n, \end{aligned} \tag{3.1}$$

where $J = 0.9$ is the Jacobian related to dissipation, and $\sigma(1)$ is a random

variable with either uniformly or normally distribution.
The map exhibits the coexistence of the period 1 and period 3 within the certain range of μ. The parameter range of this bistability depends on noise. At the threshold value of noise the period-3 attractor undergoes SNB where it dies. Figure 3.1 shows the dependence of this threshold value ξ_{th}, on parameter μ. For noise with uniform distribution (curve 2), this dependence has a minimum at $\xi_{th} = 0.0057$ for $\mu_0 = 1.084$, and a maximum at $\xi_{th} = 0.0522$ for $\mu_0 = 0.96$, whereas for noise with normal distribution (curve 1), a minimum is observed at $\xi_{th} = 0.00165$ for $\mu_0 = 1.09$, and a

maximum at $\xi_{th} = 0.0158$ for $\mu_0 = 0.97$. One can see that the period-3 attractor is more stable for $\mu_0 = 0.97$ and less stable for larger values. Normal noise destroys the attractor more easily than uniform noise.

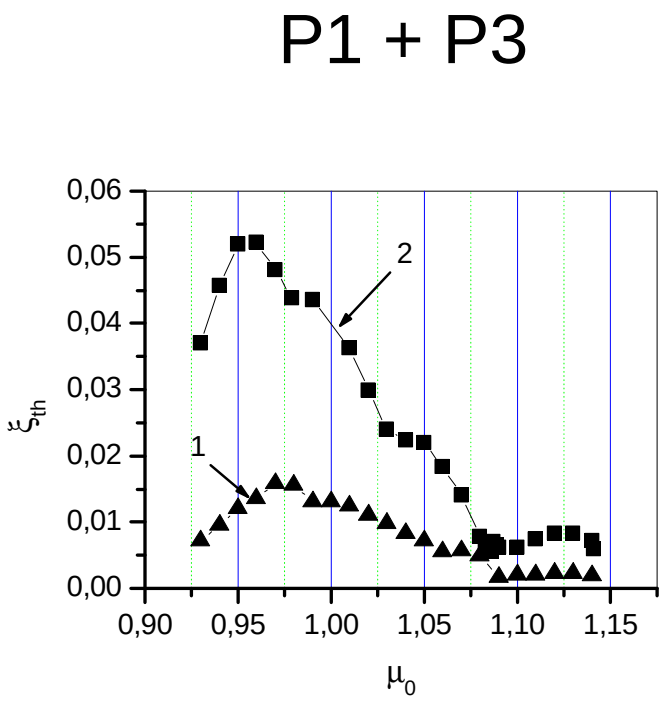

Figure 3.1: Threshold noise for annihilation of period-3 attractor in the Hénon map as a function of parameter μ_0 for (1) normal noise and (2) uniform noise.

Since each attractor has its own characteristic frequency, it becomes possible to act selectively on the desired attractor by modulating a system parameter with a properly chosen frequency. The control is applied in the form of harmonic modulation

$$\mu = \mu_0[1 + \mu_c \sin(2\pi f_c n)], \tag{3.2}$$

where μ_c and f_c are the amplitude and frequency of the control. I choose the initial value of the control parameter $\mu_0 = 1.09$ that corresponds to minimum amplitude ξ_{th} of noise with normal distribution.
Figure 3.2 demonstrates that external noise can stabilize the period-3 attractor when the modulation frequency is close to the period-doubling frequency for the period-3 attractor, i.e. $f_c \approx 1/6$.

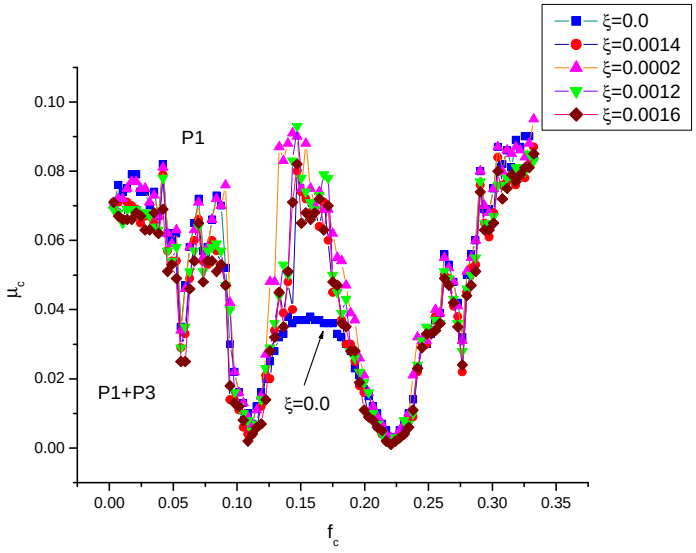

Figure 3.2: Annihilation curves for different noise levels. Noise stabilizes the period-3 attractor at certain frequencies of external modulation.

3.1.2 Noise is added to both variables

In the following I study the influence of normal noise applied to both variables and search for the threshold noise for attractor annihilation.

Let us consider the noisy Hénon map described as

$$\begin{aligned} x_{n+1} &= 1 - \mu x_n^2 + y_n + \xi\sigma(1), \\ y_{n+1} &= -Jx_n + \xi\rho(1), \end{aligned} \tag{3.3}$$

where $J = 0.9$ is the Jacobian related to dissipation, $\sigma(1)$ and $\rho(1)$ are random variables with Gaussian probability distribution of zero mean and unit standard deviation.
The annihilation curve for the period-3 attractor is plotted in figure 3.3 in the space of μ and ξ.

One can see the minimum at $\xi_{th} = 0.00113$ for $\mu = 1.095$ and the maximum at $\xi_{th} = 0.0096$ for $\mu = 0.97$. Thus, the noise effect is different for different values of the parameter μ. For $\mu = 0.97$ the period 3 is more stable.

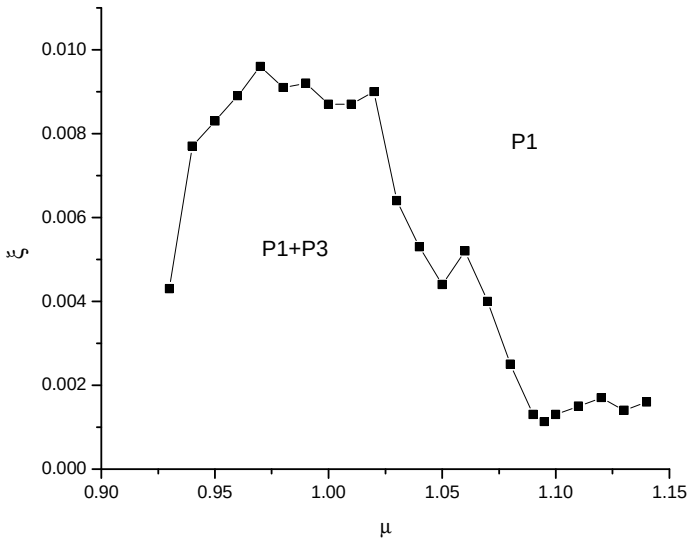

Figure 3.3: Threshold noise for annihilation of the period-3 attractor in the Hénon map with normal noise added to both variables as a function of the parameter.

Parameter modulation

I apply harmonic modulation to the parameter μ (equation 3.3). The initial value of the control parameter is $\mu_0 = 1.095$.
The threshold noise ξ_{th} for annihilation of the period-3 attractor as a function of the control frequency is shown in figure 3.4.

One can see from the figure that for higher modulation frequencies noise is not so efficient as for lower frequencies. The effect of noise for attractor annihilation is most notable for $f_c = 0.02$.
In figure 3.5 I show the annihilation curves for the period-3 attractor in the space of the control frequency and amplitude for $\mu_0 = 1.095$. Figure 3.5 demonstrates that external noise destabilizes the period-3 attractor when the modulation frequency is close to the period-doubling frequency for the period-3 attractor, i.e. $f_c \approx 1/6$.

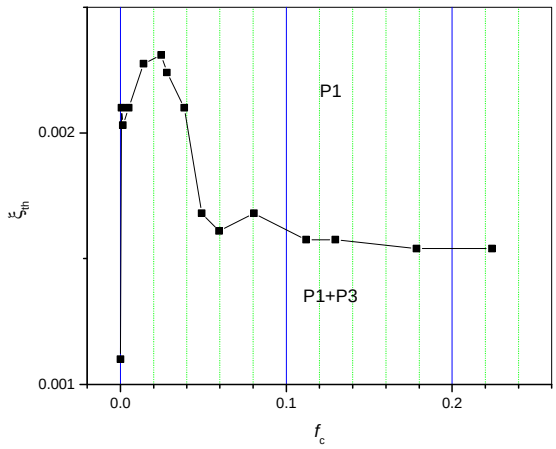

Figure 3.4: Annihilation curve for the period-3 attractor in the space of the control frequency and threshold noise for $\mu_0 = 1.095$.

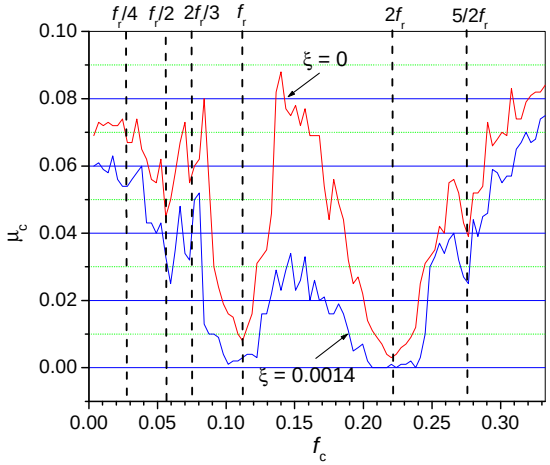

Figure 3.5: Annihilation curves for the period-3 attractor in space of the control frequency and amplitude for $\mu_0 = 1.095$.

Basins of attraction of coexisting period-1 and period-3 attractors

The basins of attraction of coexisting period-1 and period-3 attractors in the Hénon map are a very rough illustration of the dynamical processes leading to attractor annihilation. The parameter modulation not only creates periodic orbits, it also changes the organization of attractors and their basins of attraction [23]. In other words, new attractors are created by parameter modulation and they have different basins of attraction. However, the changes in the attractor boundaries have no effect on general interpretation of the phenomenon [23].

The basins of attraction of the Hénon map without harmonic modulation and without noise are shown in figure 3.6.

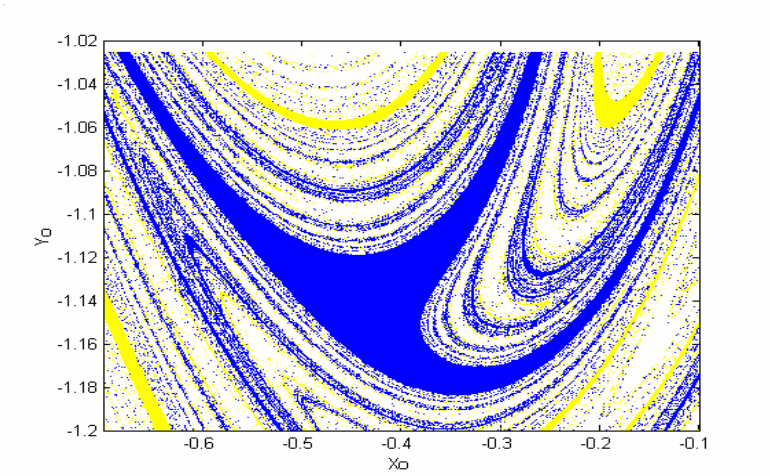

Figure 3.6: Basins of attraction of the period-1 (yellow dots) and period-3 (blue dots) attractors without control modulation and without noise for $\mu_0 = 1.095$.

Now I apply the control modulation at the relaxation oscillation frequency for the period 3, i.e. $f_c = 0.11$. The basins of attraction of the Hénon map without noise for the modulation amplitude $\mu_c = 0.0079$, is shown in figure 3.7.
One can note the decrease of the volume of the basin of the period-3 attractor in the presence of modulation $\mu_c = 0.0079$.

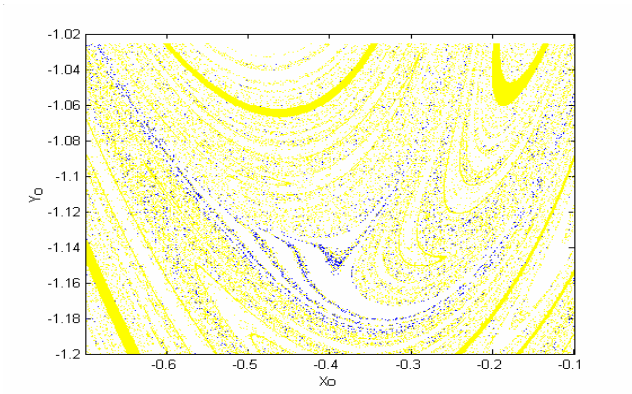

Figure 3.7: Basins of attraction of the period-1 (yellow dots) and period-3 (blue dots) attractors with modulation at $\mu_c = 0.0079$ and $f_c = 0.11$ without noise for $\mu_0 = 1.095$.

Now I apply the modulation amplitude $\mu_c = 0.0079$ and fix the frequency at $f_c = 0.11$ and study the dependence of the basin's volumes on noise. The basins with noise $\xi = 0.00325$ and modulation are shown in figure 3.8.

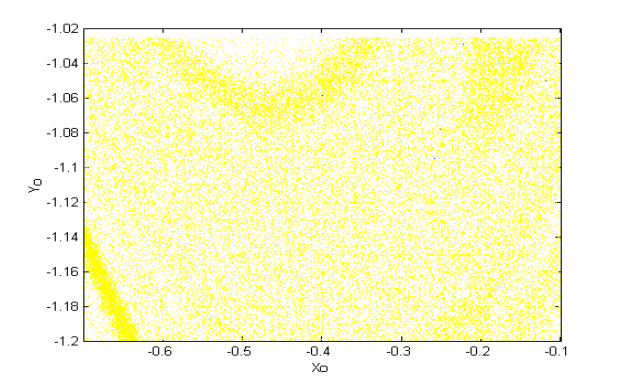

Figure 3.8: Basins of attraction of the period-1 (yellow dots) and period-3 (blue dots) attractors with modulation at $\mu_c = 0.0079$ and $f_c = 0.11$ and noise $\xi = 0.00325$.

The figure 3.8 show that noise facilitates the annihilation of the period-3 attractor.

Generalized coherence resonance

Now I change the parameter μ and consider how the basin's volumes depend on the parameter of the control modulation. The modulation is applied in the following form:

$$\mu = \mu_0 + \mu_c \sin(2\pi f_c n), \tag{3.4}$$

where μ_c and f_c are the amplitude and frequency of the control and $\mu_0 = 1.04$.
Figure 3.9 shows the basin's volumes of the coexisting period-1 and period-3 attractors as a function of the noise amplitude ξ for different values of the modulation frequency f_c. The modulation amplitude is fixed at $\mu_c = 0.02$. N is the number of initial conditions for attracting the trajectory to one of two coexisting attractors. It is seen the maximum in the volume of the basin of the period-1 for noise amplitude $\xi = 0.01$.

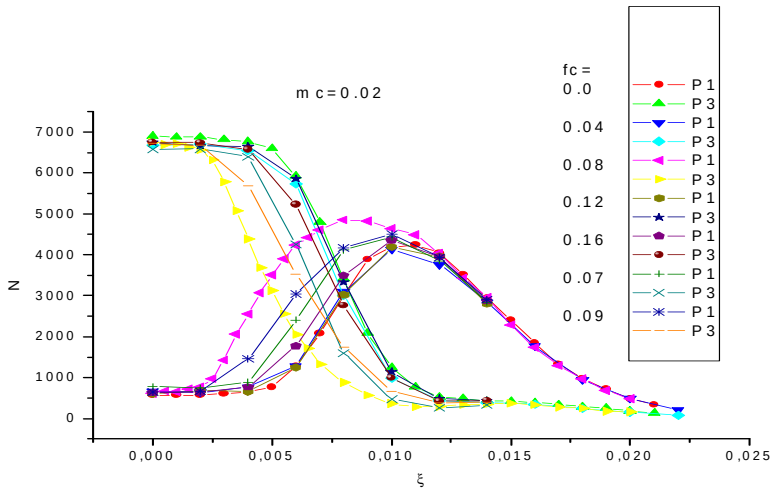

Figure 3.9: Volumes of basins of attraction of period-1 and period-3 attractors as a function of noise for different modulation frequencies at $\mu_c = 0.02$.

This figure shows the existence of a resonance in the basin's volumes that is refer to as *generalized coherence resonance.* This resonance means that noise gives a preference to one attractor over the others and so provides coherent properties of the system.

3.1.3 Discussions.

The resonant behavior of the basin's volumes results from the phenomenon of *coherence resonance*. In the case of a bistable (or multistable) system, each attractor is most sensitive to the frequency components in the noise power spectrum that remains close to the natural frequency of the attractor (eigenfrequency). In other words, the system amplifies the modulation signal (or noise components) with natural frequency (for example, $f_r = 0.08$ for the period-3 attractor). As was already mentioned above, the external modulation with a frequency close to the natural frequency of the attractor can annihilate the corresponding attractor. So, the system selects this frequency in the noise spectrum and amplifies this noise component. In this sense noise acts as an external periodic modulation, i.e. noise creates an eigenfrequency in the system. With increasing noise amplitude, this frequency destroys the basin of attraction of one of the attractors (period 3) while the volume of the basin of the other coexisting attractor (period 1) is increased. However, the volume of the basin cannot increase infinitely. Instead, it reaches maximum at a certain noise level. Finally, high noise destroys all attractors together with their basins, as one can see in figure 3.9. We refer this resonance to as *generalized coherence resonance*, because it appears only in systems demonstrating generalized multistability [24].

3.2 Coexisting periodic and chaotic orbits

In this chapter I study the Hénon map in the parameter region where the period-3 attractor and the chaotic attractor coexist. I explore the range of the coexistence of the period-3 and chaotic attractors and apply small harmonic modulation to the control parameter while the system stays either in the period-3 state or in chaos.
Figure 3.10 shows the bifurcation diagram of the Hénon map with coexisting period-3 and chaotic attractors at interval $\mu = (1.62, 1.65)$.

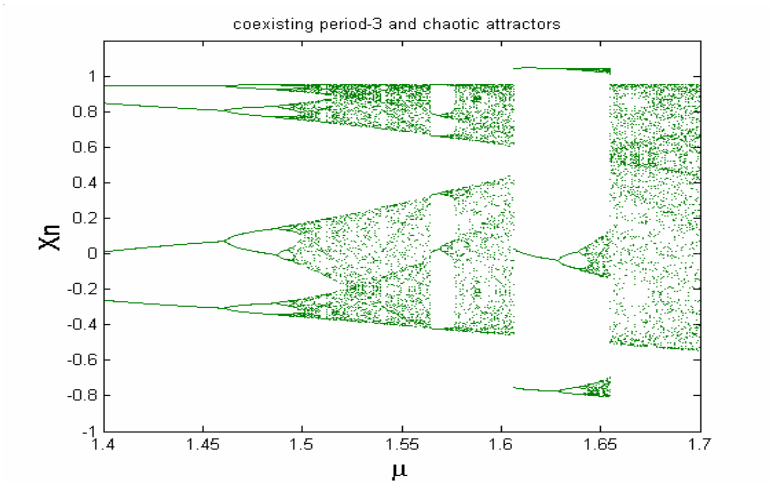

Figure 3.10: Bifurcation diagram of the Hénon map with coexisting period-3 and chaotic attractors .

3.2.1 Modulation is applied while the system stays in the period-3 attractor

The Hénon map with noise is described as

$$\begin{aligned} x_{n+1} &= 1 - \mu x_n^2 + y_n + \xi\sigma(1), \\ y_{n+1} &= -Jx_n + \xi\rho(1), \end{aligned} \tag{3.5}$$

where $J = 0.06$ and $\sigma(1)$ and $\rho(1)$ are random variables with Gaussian probability distribution of zero mean and unit standard deviation.

The control is applied in the form of harmonic modulation

$$\mu = \mu_0 + \mu_c \sin(2\pi f_c n), \tag{3.6}$$

where μ_c and f_c are the amplitude and frequency of the control. $\mu_0 = 1.62$.

Figure 3.11 shows the annihilation curves for the period-3 attractor in the space of the control frequency and amplitude for different noise levels.

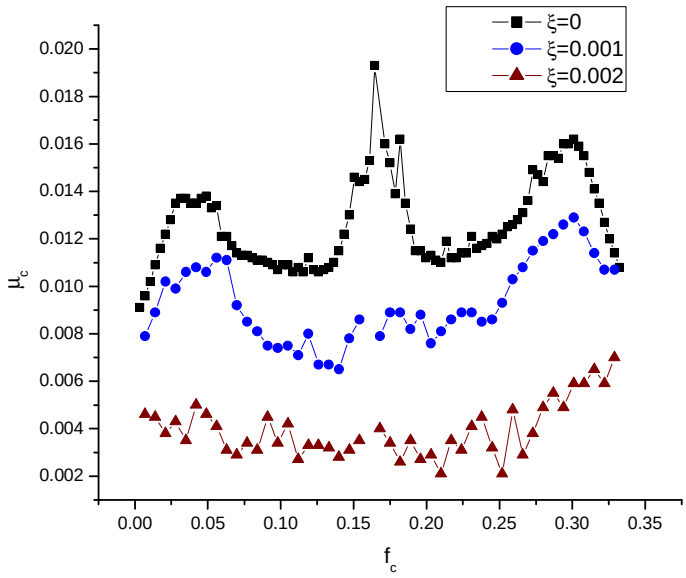

Figure 3.11: Annihilation curves for period-3 attractor in space of control frequency and amplitude for different noise levels.

3.2.2 Modulation is applied while the system stays in chaos.

In this section I study the Hénon map with coexisting period-3 and chaotic attractors. I analyze the power spectra and measure SNRs. The SNR has a maximum at resonance frequency f_r. This is called *deterministic resonance*. In a noisy nonchaotic system this phenomenon is called *stochastic resonance*. In the presence of both, chaos and noise, this resonance phenomenon is referred to as *deterministic stochastic resonance* and the resonance frequency f_r depends on the noise level as shown in figures 3.12 and 3.13.
In figure 3.12 I plot the dependences of the resonance frequency f_r(SNR) on the modulation amplitude for different noise values.

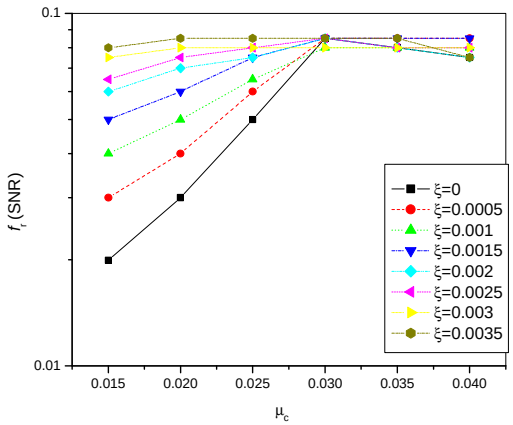

Figure 3.12: f_r (SNR) dependence in the modulation amplitude μ_c, for different noise values.

In figure 3.13 I show how the resonance frequency f_r(SNR) depends on noise for different control amplitudes.

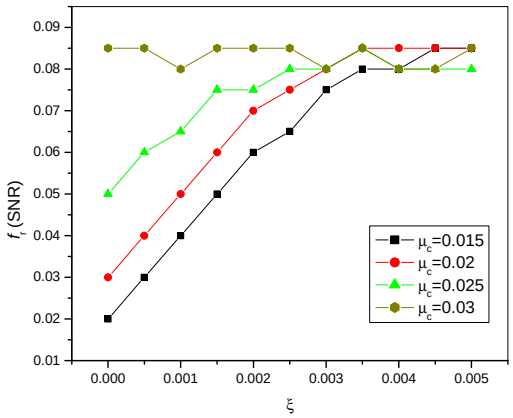

Figure 3.13: Resonance frequency f_r(SNR) versus noise for different modulation amplitudes.

From both figures I can conclude that the resonance frequency increases approximately exponentially with increasing the modulation frequency and linearly with noise for small amplitudes and small noise, and saturates approaching the frequency of relaxation oscillations (or natural frequency) of the period-3 attractor, i.e. $f_r(\text{SNR}) = f_r^{(3)}$, for large amplitudes and noise.

3.2.3 Discussions.

In the volumes of the basins of attraction of coexisting attractors, I have found that the system amplifies the modulation signal (or noise components) with natural frequency (for example, the natural frequency for the period-3 attractor $f_r^{(3)} = 0.08$). When the noise level is increasing, the volume of the basin of attraction of the period-1 attractor is growing, while the volume of the basin of the period-3 attractor is decreasing. At a certain level of noise the volume of the basin of the period-1 attractor reaches a maximum value and with a further increase in the noise level, the volumes of both basins decrease. As was already mentioned we refer to this effect as *generalized coherence resonance*, because it appears only in systems demonstrating generalized multistability [24]. I have studied the power spectra of the Hénon map in the region with coexisting period-3 and chaotic attractors and I have not found *deterministic resonance* and also, I have not found *deterministic-stochastic resonance*.

Chapter 4

Control of multistability in an erbium-doped fiber laser with pump modulation.

Introduction

Erbium-doped fiber lasers (EDFLs) are widely used in many areas of science and technology, including communications, reflectometry, sensing, and medicine, due to their exclusive advantages of high gain and a single transversal mode operation. These laser are also interesting from a point of view of nonlinear dynamics because of their high sensitivity to any external perturbation which can destabilize their normal operation so that the laser oscillates in a nonlinear regime. Therefore the knowledge of a dynamic behavior of the EDFLs under external modulation is of great importance not only for their technological application, but also for fundamental research in nonlinear dynamics [26].

In this chapter I study complex dynamics of an erbium-doped fiber laser subject to harmonic modulation of a diode pump laser. I use a novel laser model developed by A.V. Kiryanov, that describes all experimentally observed features reported by Pisarchik *et al.* [27].

The coexistence of different regimes is demonstrated with codimensional-one and codimensional-two bifurcation diagrams in parameter space of the modulation frequency and amplitude.

4.1 Theory

4.1.1 Laser Dynamics.

A laser is usually classified according to the material that provides optical amplification. This material determines largely the properties of the laser: the mode of operation (pulsed or continuous), the emission wavelength, the output power/energy and the coherence properties. Gaseous, liquid, solid state fiber can provide optical amplification when is properly excited. The laser transition of the amplifying material may be homogeneously broadened, i.e., the light of a certain optical frequency can interact with all atom/molecules, all of them having the same resonance frequency. A homogeneous line width $\triangle v_H$, is given by the medium relaxation rates:
$\gamma_\perp + \gamma_\parallel = \pi \triangle v_H$
, where $\gamma_\perp$ and $\gamma_\parallel$ are the relaxation rates for inversion and polarization, respectively. In a inhomogeneous broadening case, the material consists of atoms/molecules of different resonance frequencies. Light of a particular optical frequency can then only interact with a fraction of the total number of atoms/molecules. Lasers may be classified in still another way. Lasers operating in a single emission mode are described by three equations for the three relevant variables: field, population and polarization. Usually, decay is measured on a very different time scale, which is given by the relaxation rates κ (damping rate of the laser resonator), $\gamma_\perp$ and $\gamma_\parallel$. If one of them is much larger than others, the corresponding variable relaxes fast and consequently adiabatically adjusts to the others. The number of equations describing the laser is then reduced.
Those lasers for which the population and polarization decay fast in comparison with the field have been called *class A lasers*; those for which only the polarization relaxes fast, *class B lasers*; and those for which all three relaxation rates are of a similar magnitude, *class C lasers*.
Laser equations for the class A laser reduce to one. Therefore, only a constant output solution exists. For the class B laser, oscillation of energy between field and inversion population is possible and the equations yield relaxation oscillations. The class C laser with their coupled dynamics of field, inversion population, and polarization can display undamped periodic or non-periodic (chaotic) pulsing.
Class B lasers can, however, show chaotic dynamics when they are externally influenced via (modulation of a parameter, injection of external light, or feedback).
A fiber laser belongs to the *class B* lasers because the polarization in this

laser can be adiabatically eliminated and the dynamics can be ruled by two rate equations for field and population inversion. The oscillations in the *class B* lasers can be observed only if an additional degree of freedom is added in the form of either saturable absorber, light injection, or external modulation. Different dynamical regimes, bistability, and chaos have been observed in the fiber laser with modulated parameters. Recently, coexistence of multiple periodic and chaotic attractors have been found numerically in an EDFL with loss modulation. The final adiabatically attracting state is determined only by initial conditions. The period of a particular periodic attractor is equal to subharmonic of the modulation frequency. Each subharmonic branch is born in a regular saddle-node bifurcation (SNB) and the optimal condition (minimal driving amplitude) for the appearance of the subsequent branch is achieved when the driving frequency is close to the corresponding harmonic of the relaxation oscillation frequency. The overlapping of the subharmonic branches results in generalized multistability (coexistence of attractors).
From the experimental point of view, the pump modulation is easier to realize than the modulation of the cavity loss. An important difference of the band on heavily-doped active laser from other class B lasers is that the former laser represents self-pulsations, i.e., this laser acts as an autonomous system. The self-pulsing behavior is usually attributed to the presence of the saturable loss due to erbium ion pairs or pump depletion in the fiber. Recently, period-doubling and quasi-periodic routes to chaos have been observed in a self-pulsing dual-wavelength EDFL. In this sense, the dynamics of the EDFL under pump modulation is more sophisticated than the dynamics of other class-B lasers.

4.2 Experimental Conditions.

The experimental setup is shown schematically in Figure 4.1.

The erbium-doped fiber laser is pumped by a commercial laser diode (wavelength $976nm$, maximum pump power 300mW) through a wavelength-division multiplexer (WDM) and a polarization controller (PC). The linear laser cavity with a 1.5nm length is formed by a piece of heavily doped erbium fiber (SCL110-01 from IPHT) having a 70 cm length and a core diameter of $2.7\mu m$ (NA O.27), and two Fiber Bragg Gratings (FBG1 and FBG2) with a 2nm full-width at half-maximum (FWHM) bandwidth and reflectivity of 91% and 95% at a 1560 nm wavelength. The active fiber has high concentration of erbium ions (about 2300 ppm) corresponding to absorption

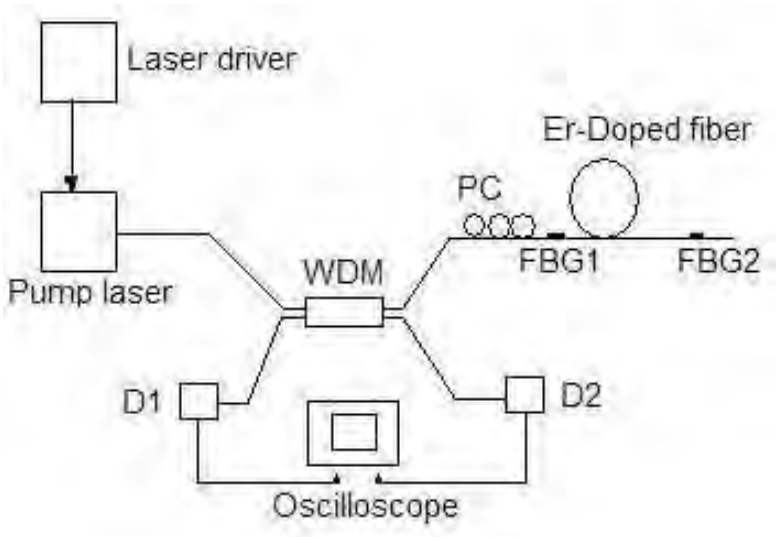

Figure 4.1: Experimental setup.WDM is the wavelength-division multiplexing coupler,PC is the polarization controller, FBG1 and FBG2 are the Bragg gratings, and D1 and D2 are the photodetectors.

of 18.5 dB/m at a 980 nm wavelength. The output power of the pumping laser diode can be modulated with a signal generator controlling the drive current. The output signals from the pump diode laser and from the fiber laser are recorded with photodetectors D1 and D2 and analyzed with an oscilloscope. The optical spectrum bandwidth of the laser is less than 0.1 nm (resolution of the spectrum analyzer).
In the absence of pump modulation, the laser generates periodic oscillations with the fundamental laser frequency (relaxation oscillations) owing to the presence of saturable loss in the fiber. The amplitude and frequency of the oscillations depend on the pump power. When the pump power is low, the response of the laser is sinusoidal, whereas at the high powers ($>$ 20mW) the fiber laser oscillates in a pulsed regime at a higher repetition rate.
In the presence of harmonic pump modulation, two competitive processes are involved in the laser dynamics. These are the self-oscillations and the external modulation. Thus, the final dynamics depends basically on the relationship between the characteristic frequencies of these two processes.
The laser dynamics is ruled mainly by the ratio of modulation frequency f to fundamental laser frequency $f_0 = 30kH$ which corresponds to the pump power of 15mW. The latter is defined by the saturable loss in the fiber and

pump power. General features of the dynamics of the EDFL subjected to pump modulation [26]. When the modulation frequency is lower than half of the fundamental laser frequency ($f < f_0/2$) a strong interaction of f with f_0 can lead to frequency and phase locking of self-pulsations to the external modulation. In this frequency range, the frequency of the laser response can be controlled by the parameter modulation. In the case of frequency locking, the ratio of the two frequencies becomes constant at a rational number. The locked regions in a plane of modulation frequency versus modulation amplitude form the Arnold's tongues and a transition to chaos via period doubling is observed. Moreover, once the ratio of f and f_0 is an irrational number, a quasi-periodic route to chaos is possible. A similar behavior has been observed in other class-B lasers with a saturable absorber and widely discussed in scientific literature. For small values of the modulation amplitude, the laser response asymptotically approaches the stable limit cycle, so is consider that the response to be linear.

4.2.1 Laser Model.

In simulations I use the laser model reported by Pisarchik *et al* [12]. The model is based on the rate equations in which a power-balance approach is applied to a longitudinally pumped EDFL, in which ESA in erbium at the $1.5\mu m$ wavelength and averaging of the population along the pumped active fiber are taken into account. An energy-level diagram of erbium is shown in Figure 4.1.

However, notice that this model does not incorporate the mechanisms

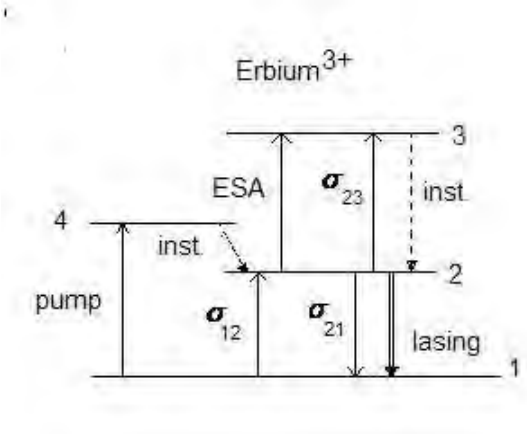

Figure 4.2: Erbium energy-level diagram.

responsible for establishing the self-pulsing regime in the laser, such as a thermo-lensing effect and erbium ion pairs, for the following reasons. First, in the experiments [27] the pump power is small to introduce thermo lensing and second, the concentration of erbium is quite low to make the effect of ion pairs significant. The balance equations for intracavity laser power P (which is a sum of the powers of the cotrapropagating waves inside the cavity, in inverse seconds) and the averaged (over the active fiber length) population N of the upper (2) level (which is a dimensionless variable, $0 \leq N \leq 1$) are

$$\frac{dP}{dt} = \frac{2L}{T_r} P\{r_w \alpha_0 [N(\xi_1 - \xi_2) - 1] - \alpha_{th}\} + P_{sp} \tag{4.1}$$

$$\frac{dN}{dt} = -\frac{\sigma_{12}\Gamma_s r_w P}{\pi r_0^2}(N\xi_1 - 1) - \frac{N}{\tau} + P_{pump} \tag{4.2}$$

where $N = (1/n_0 L) \int N_2(z)dz$ (N_2 is the population of upper laser level 2, n_0 is the refractive index of a cold erbium-doped fiber core, and L is the active fiber length) and σ_{12} is the cross section of the absorption transition from ground state 1 to upper state 2. Here we assume that the cross section of the return stimulated transition is practically the same ($\sigma_{12} = \sigma_{21}$) yielding $\xi_1 = (\sigma_{12} + \sigma_{21})/\sigma_{12} = 2$. $\xi_2 = \sigma_{23}/\sigma_{12} = 0.4$ is the coefficient that stands for the ratio between the ESA (σ_{23}) and groundstate absorption cross sections at the laser wavelength, $T_r = (2n_0/c)(L + l_0)$ is the photon intracavity round-trip time [l_0 is the total length of the fiber Brag grating(FBG) coupler tails inside the cavity], $\alpha_0 = N_0\sigma_{12}\Gamma_s$ is the small-signal absorption of the erbium fiber at the laser wavelength ($N_0 = N_1 + N_2$ is the total concentration of erbium ions in the active fiber and Γ_s is the overlap factor for EDFL radiation), $\alpha_{th} = \gamma_0 + (1/2L)In(1/R)$ is the intracavity loss on threshold (γ_0 is the nonresonant fiber loss and R is the total reflection coefficient of the FBG couplers), τ is the lifetime of erbium ions in excited state 2, r_0 is the fiber core radius, w_0 is the radius of the fundamental fiber mode, and $r_w = 1 - exp[-2(r_0/w_0)^2]$ is the factor that addresses a match between the laser fundamental mode and erbium-doped core volumes inside the active fiber in Equation 4.1, $P_{sp} = N(\frac{\lambda_g}{w_0})^2 \frac{r_0^2 \alpha_0 L}{4\pi^2 \sigma_{12}\Gamma_s \tau T_r}x10^{-3}$ is the spontaneous emission into the fundamental laser mode. It is assumed that the laser spectrum width is 10^{-3} of the erbium luminescence spectral bandwidth (λ_g is the laser wavelength). In Equation 4.2, $P_{pump} = (P_P/N_0\pi r_0^2 L)1 - exp[-\alpha_p L(1 - N)]$ is the pump power, where P_p is the pump power at the fiber entrance and $\alpha_p = N_0\sigma_{14}\Gamma_p$ is the small-signal absorption of the erbium fiber at the pump wavelength (σ_{14} is the cross section of the absorption transition from level 1 to level 4

and Γ_p is the overlap factor for pump radiation). The system of Equations 4.1 and 4.2 describes the laser dynamics without external modulation. The harmonic pump modulation is added as

$$P_p = P_P^0[1 + m\sin(2\pi F_m t)] \tag{4.3}$$

where m and F_m are the modulation depth and frequency, respectively, and P_P^0 is the pump power without modulation (at $m = 0$). The calculations are performed for the experimental conditions described in Table 4.1.

The value of w_0 has been measured experimentally, being slightly higher

Table 4.1: Parameters used in simulations

Parameter	Dimension	Value
L	cm	70
n_0		1.45
l_0	cm	20
T_r	ns	8.7
r_0	cm	$1.5\text{x}10^{-4}$
τ	s	10^{-2}
w_0	cm	$3.5\text{x}10^{-4}$
σ_{12}	cm^2	$2.3\text{x}10^{-21}$
σ_{23}	cm^2	$0.9\text{x}10^{-21}$
σ_{14}	cm^2	$0.46\text{x}10^{-21}$
γ_0		0.038
R		0.8
N_0	cm^{-3}	$5.4\text{x}10^{19}$
α_0	cm^{-1}	0.0534
α_p	cm^{-1}	0.025

than the value $2.5\text{x}10^{-4}cm$ given by the formula for a step-index single-mode fiber: $w_0 = r_0(0.65 + 1.619/V^{1.5} + 2.879/V^6)$ where V is related to numerical aperture NA and r_0, as $V = (2\pi r_0/\lambda_g)NA$; the values r_0 and w_0 result in $r_w = 0.308$. The coefficients α_0 and α_p characterizing the resonant-absorption properties of the erbium fiber at the laser and pump wavelengths, were measured directly in the heavily doped fiber with $\Gamma_s = 0.43$ and $\Gamma_p = 1$. The values γ_0 and R yield $\alpha_{th} = 3.92$ x 10^{-2}. The lasing wavelength is taken to be $\lambda_g = 1.56$ x 10^{-4}cm ($h\nu_g = 1.274\text{x}10^{-19}J$), corresponding to the maximum reflection coefficients of the FBGs centered on this wavelength. The parameters which can be varied in experiments are (i) the excess over the first laser threshold, $\epsilon = P_r/P_{th}$, where the threshold pump

power, $P_{th} = N_{th}(N_0 L\pi w_p^2/\tau)\{1 - exp[-\alpha_p L(1 - N_{th})]\}^{-1}$ and the threshold population of level 2 is $N_{th} = (1/\xi_1)[1 + (\alpha_{th}/r_w\alpha_(0))]$, (the radius of the pump beam was taken, for simplicity, the same as the one of the laser beam, , $w_0 = r_g$) and (ii) the parameters of pump modulation: modulation frequency F_m and modulation depth m.

4.2.2 Normalized equations.

To simplify and generalize the laser model, we transform the complete system of Equations 4.1 and 4.2 with a normalization.
Transforming these equations ($\frac{dP}{dt} = \frac{2L}{T_r}P\{r_w\alpha_0[N(\xi_1 - \xi_2) - 1] - \alpha_{th}\} + P_{sp}$

$\frac{dN}{dt} = -\frac{\sigma_{12}\Gamma_s r_w P}{\pi r_0^2}(N\xi_1 - 1) - \frac{N}{\tau} + P_{pump})$
where:
1. $P_{pump} = P_p[\frac{\{1-exp[-\alpha_p L(1-N)]\}}{N_0\pi r_0^2 L}]$
2. $P_{sp} = N(\frac{\lambda_g}{w_0})^2\frac{r_0^2\alpha_0 L}{4\pi^2\sigma_{12}\Gamma_s\tau T_r}\text{x}10^{-3}$
3. $\alpha_{th} = \gamma_0 + (\frac{1}{2L})\ln\frac{1}{R}$
4. $T_r = (2n_0/c)(L + L_0)$
5. $r_w = 1 - exp[-2(\frac{r_0}{w_0})^2]$

we can arrive to their simpler form

$$\frac{dx}{d\theta} = axy - bx + c(y + r_w) \tag{4.4}$$

$$\frac{dy}{d\theta} = -dxy - (y + r_w) + e\{1 - e[-\alpha_p L(1 - \frac{y + r_w}{\xi_1 r_w})]\} \tag{4.5}$$

where the following changes have been made in the variables:

$$x = \frac{P}{\gamma} \tag{4.6}$$

$$y = r_w[\xi_1 N - 1] \tag{4.7}$$

$$\theta = \frac{t}{\tau} \tag{4.8}$$

and in the parameters:

$$a = 2L(\frac{\tau(\xi_1 - \xi_2)\alpha_0}{\tau_r\xi_1}) \tag{4.9}$$

$$b = -[2L(\frac{\tau}{T_r})(\frac{-\xi_2\alpha_0 r_w}{\xi_1} - \alpha_{th})] \tag{4.10}$$

$$c = \frac{\tau}{\xi_1 r_w} \tag{4.11}$$

$$d = \frac{\tau\xi_1 r_w \sigma_{12}\Gamma_s\gamma}{\pi r_0^2} \tag{4.12}$$

$$e = P_p[\frac{\tau\xi_1 r_w}{N_0 L\pi r_0^2}]. \tag{4.13}$$

The variables x and y are now for the normalized laser power density and inversion population, respectively. The values of the new parameters are presented in Table 4.2.

Table 4.2: Nomalized Parameters used in simulations

Parameter	Value
a	6.6207x 10^7
b	7.365517x10^6
c	0.0163
d	4.077x10^3
e	506

4.3 Numerical results.

The numerical calculations employing the system of equations 4.1 and 4.2 or 4.4 and 4.5 allow us to obtain time series and bifurcation diagrams for characterization of the dynamics of the pump-modulated EDFL. As was shown previously, the dynamics of this laser, as well as of other class-B lasers, is related to the main laser resonance, which appears close to the relaxation oscillation frequency of the laser, f_0. A rich variety of attractors arises in primary saddle-node bifurcations(SNBs). Depending on the modulation frequency, the laser response may contain either subharmonics or higher harmonics of F_m. At the high-frequency range ($F_m > f_0$) various SNBs give rise to subharmonic laser oscillations, whereas at the relatively low modulation frequencies ($F_m < f_0$) the higher harmonics of F_m rule the laser dynamics. The dynamics of the pump-modulated EDFL in the high-frequency range has been investigated experimentally [26].

We address here only the numerical results obtained at the high-frequency range.
Codimensional-one bifurcation diagrams. This diagram is constructed by slowly increasing and decreasing the control parameter. The coexistence of two and three attractors is clearly seen in the figures 4.3 and 4.4. In

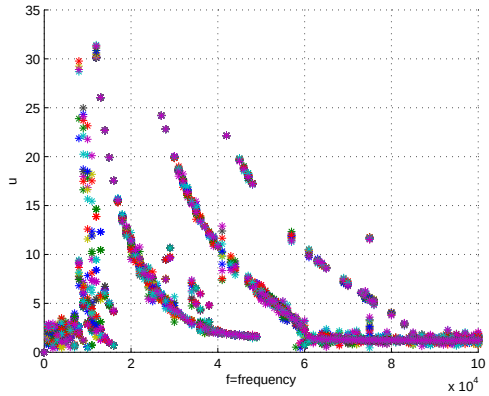

Figure 4.3: Bifurcation diagrams of peak laser intensity with driving frequency as control parameter at $A_d = 0.7V$.

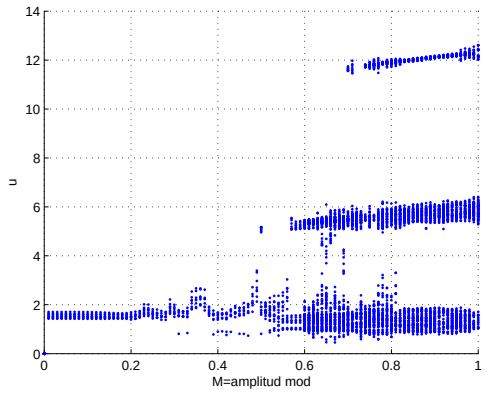

Figure 4.4: Bifurcation diagrams of peak laser intensity with driving amplitude as a control parameter at $f_d = 75kHz$.

figure 4.5 the f_c spectral component is plotted, S_c, in the power spectrum of the laser output versus the control frequency for the laser oscillating in

the period-3 and period-4 regimes at $A_c = 0.007$. One can see that the resonance frequency for the period-4 attractor is $2kHz$ and for the period-3 is $3kHz$.

As A_c is increased, the laser response to the control modulation becomes

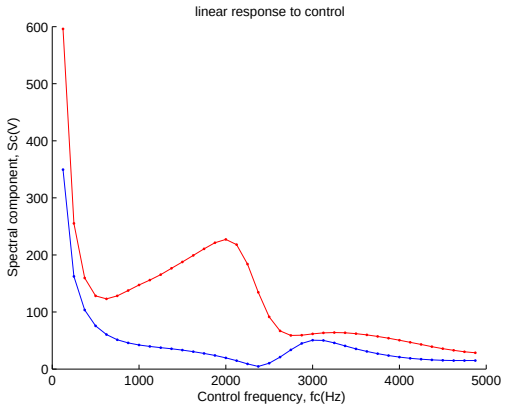

Figure 4.5: Linear laser responses to control modulation with $A_c = 0.007$ at $f_d = 75$ and $A_d = 0.7$.

nonlinear that leads to the attractor annihilation.

Figure 4.6 shows time series demonstrating coexistence of different dynamical regimes at $Fd = 70.2$ and $Ad = 0.8$. The lower trace shows the pump modulation signal.

Figure 4.7 shows the codimension-two bifurcation diagram in (fc, Ac) parameter space at $Ad = 0.8$ and $Fd = 70.2$. The curve connecting the green with black and red region is the crisis line (the annihilation curve) for the period-1 and period-3 attractors, respectively.

Figure 4.8 shows codimension-two bifurcation diagram in (fc, Ac) parameter space at $Ad = 0.8$ and $Fd = 70.2$. The curve connecting the black with red region is the crisis line (the annihilation curve) for the period-1.

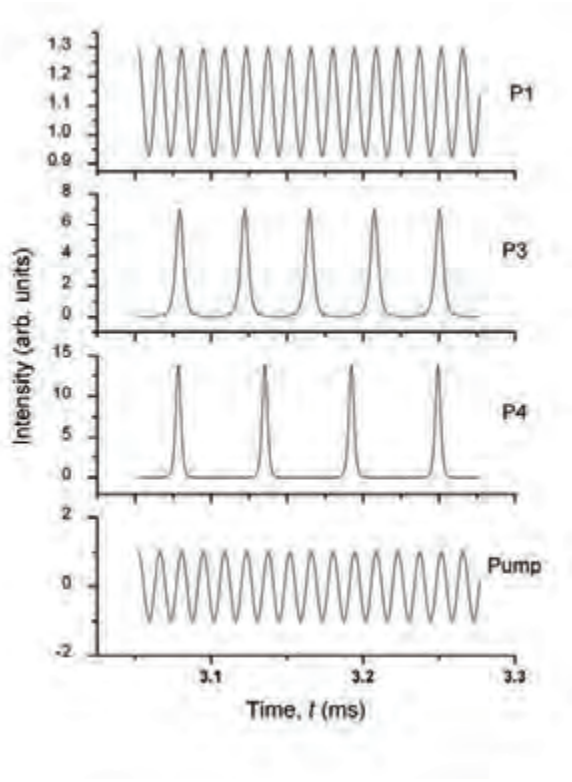

Figure 4.6: Time series demonstrating coexistence of different dynamical regimes at $Fd = 70.2$ and $Ad = 0.8$. The lower trace shows the pump modulation signal.

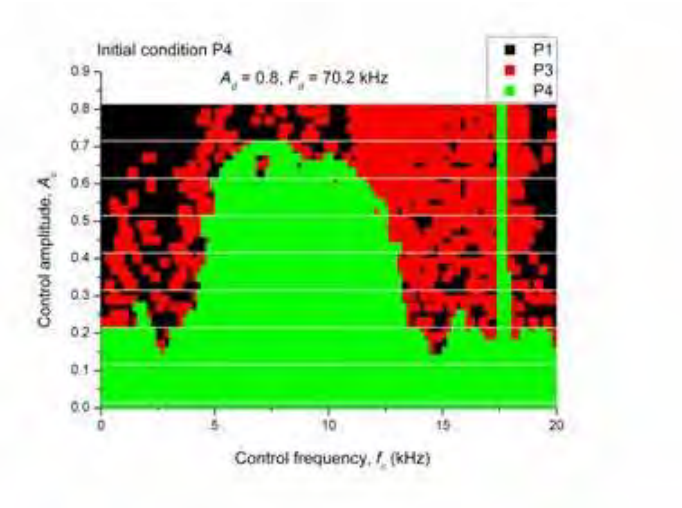

Figure 4.7: Codimension-two bifurcation diagram in (fc, Ac) parameter space at $Ad = 0.8$ and $Fd = 70.2$. The curve connecting the green with black and red region is the crisis line (annihilation curve) for the period-1 and period-3 attractors, respectively.

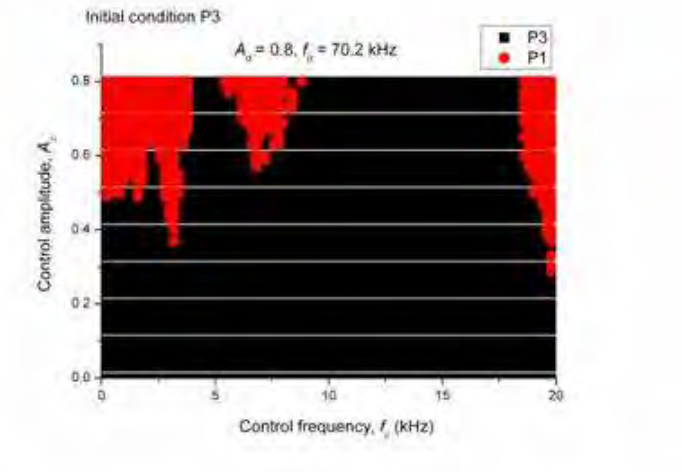

Figure 4.8: Codimension-two bifurcation diagram in (fc, Ac) parameter space at $Ad = 0.8$ and $Fd = 70.2$. The curve connecting the black with red region is the crisis line (annihilation curve) for the period-1.

Chapter 5

Conclusions.

In this thesis I have demonstrated the applicability of the method for attractor annihilation in a multistable system subject to noise. I have shown with the noisy Hénon map, that additive noise can either enhance or worsen the efficiency of attractor annihilation, depending on the control parameters. Therefore, noise can be used for both stabilization and destabilization of coexisting attractors in a multistable system. The noise-induced resonance phenomenon (generalized coherent resonance) has been found in the volumes of the basins of coexisting attractors.

I have also investigated numerically dynamics of an erbium-doped fiber laser subject to parameter modulation of the diode pump laser. I have demonstrated annihilation of one or two coexisting attractors in the laser with three periodic attractors. The results of simulations are in good agreement with experiments reported previously by Pisarchik et al.

I believe that the described phenomena can be observed in other dynamical systems with coexisting attractors. The results of the present thesis can be useful in other areas of science where a multistable behavior takes place.

Bibliography

[1] A.N. Pisarchik and B.K. Goswami, Annihilation of one of the coexisting attractors in a bistable system, Phys. Rev. Lett. **84** (2000) 1423-1426.

[2] A.N. Pisarchik, Oscillation death in coupled nonautonomous systems with parametrical modulation, Phys. Lett. A **318** (2003) 65-70.

[3] B.E. Martínez-Zerega, A.N. Pisarchik, and L. Tsimring, Using periodic modulation to control coexisting attractors induced by delayed feedback, Phys. Lett. A **318** (2003) 102-111.

[4] A.N. Pisarchik and B.F. Kuntsevich, Control of multistability in a directly modulated diode laser, IEEE J. Quantum Electron. **38** (2002) 1594-1598.

[5] A.N. Pisarchik, Yu.O. Barmenkov, and A.V. Kir'yanov, Experimental demonstration of attractor annihilation in a multistable fiber laser, Phys. Rev. E **68** (2003) 066211.

[6] T. Wellens, V. Shatokhin, and A. Buchleitner, Stochastic resonance, Reports on Progress in Physics **67** (2003) 45-105.

[7] Priya Ranjan and Eyad H. Abed, Enhancing Detectability of Bifurcations in DC-DC Converters by Stochastic Resonance, Proceedings of the 39"' IEEE Conference on Decision and Control. Sydney, Australia December, 2000, pp. 1608-1612.

[8] E. Lacot, F. Stoeckel, and M. Chenevier, "Dynamics of an erbium-doped fiber laser", Phys. Rev. A **49**, 3997-4008(1994).

[9] F. Sanchez, M. LeFlohic, G.M. Stephan, P. LeBoudec, and P.L. Francois, "Quasi-periodic route to chaos in erbium-doped fiber laser", IEEE J. Quantum Electron. **31**, 481-488(1995).

[10] L. Luo, T.J. Tee, and P.I. Chu, "Chaotic behavior in erbium-doped fiber-ring lasers" J. Opt. Soc. Am. B **15**, 972-978(1998).

[11] Q. Mao and J.W.Y. Lit, "Optical bistability in an L-band dual-wavelength erbium-doped fiber laser with overlapping cavities" IEEE J. Quantum Electron. **14**, 1252-1254(2002).

[12] A.N.Pisarchik, Yu. O. Barmenkov, A.V.Kir'yanov, and R.Jaimes-Retegui, *Dynamics of an erbium-doped fiber laser with pump modulation:theory and experiment.* Opt. Soc. Am. B, Vol.**22**, No. 10, 2107 (2005).

[13] J.M.T. Thomson and H.B. Stewart, *Nonlinear Dynamics and Chaos*, ed. John Wiley, Chichester,1988.

[14] S.N. Elaydi, *Discrete Chaos*, ed. CHAPMAN & HALL/CRC, Boca Raton, 2000.

[15] K.T. Alligood, T.D. Sauer and J.A. Yorke, *Chaos: An Introduction to Dynamical Systems*, ed. Springer, New York, 2000.

[16] R. Jaimes Reategui, *Dynamic of Complex Systems with Parametric Modulation: Duffing Oscillators and a Fiber Laser*, PhD Thesis, Centro de Investigaciones en Optica, Leon, Gto., Mexico, 2004.

[17] B.E. Martínez Zérega, *Laser Applications: Controlling Multistability in Dynamical Systems with Delay Feedback*, PhD Thesis, Centro de Investigaciones en Optica, Leon, Gto., Mexico, 2005.

[18] M.Digonnet, ed., *Rare Earth Doped Fiber Lasers and Amplifiers* (Marcel Dekker, 1993).

[19] R. Benzi, A. Sutera, and A. Vulpiani, "The mechanism of stochastic resonance," J. Physics A: Math. and General, vol. 14, pp. L453–L457, (1981).

[20] B. McNamara and K. Wiesenfeld, Theory of stochastic resonance,Phys. Rev. A vol **39, No. 9,** 4854 (1989).

[21] V. S. Anishchenko, A. B. Neiman, and M. A. Safonova,"Stochastic resonance in chaotic systems," J. Statist. Physics, vol. 70, nos. 1/2, pp. 183–196, (1993).

[22] B. Linder and L. Schimansky-Geier, Coherence and stochastic resonance in a two-state system, Phys. Rev. E **61** (2000), 6.

[23] A.N. Pisarchik, Controlling the multistability of nonlinear systems with coexisting attractors, Phys. Rev. E **64 (**2001) 046203.

[24] C.Yu. Calderón-Hermosillo and A.N. Pisarchik, Generalized coherence resonance, Conference *Latinoamericanas en las Ciencias Exactas de la Vida Mujer Ciencia 2006*, May 3-5, 2006, Mexico D.F, Memorias pp. 90.

[25] C.O. Weiss and R. Vilaseca, Dynamics of lasers. Weinheim: VCH, 1991.

[26] A.N.Pisarchik, Yu. O. Barmenkov, and A.V.Kir'yanov, "Experimental characterization of bifurcation structure in an erbium-doped fiber laser with pump modulation.", IEEE J. Quantum Electron. **39**, 1567-1571 (2003).

[27] A.N.Pisarchik, Yu. O. Barmenkov, and A.V.Kir'yanov, "Experimental demostration of attractor annihilation in a multistable fiber laser.", Phys. Rev. E **68**, 066211(2003).

[28] C.Yu. Calderón-Hermosillo and A.N. Pisarchik, Attractor annihilation in the noisy Hénon map, *III Encuentro Participación de la Mujer en la Ciencia,* May 18-19, 2006, Leon, Gto., Mexico, Memorias pp. 33.